Ultra-Wideband Quad Element MIMO Antenna on a Flexible Substrate for 5G and Wearable Applications

Achari P. Abhilash[1, *], Karamkulambel K. Indhu[1], Ramakrishnan Anil Kumar[1], Kinatingal Neema[1], and Chandroth K. Aanandan[2]

Abstract—This study describes the development of a low-profile, omnidirectional, CPW-fed Ultra-Wide Band (UWB) MIMO antenna. The antenna is designed on a flexible FR4 substrate with thickness $0.07\,\mathrm{mm}$, making it suitable for wearable applications. The fractional bandwidth obtained is more than 100% (3.1–$9.3\,\mathrm{GHz}$) which spans the wireless communication bands such as ISM (5.15–$5.35\,\mathrm{GHz}$), ISM (5.725–$5.825\,\mathrm{GHz}$), Wi-Fi ($5\,\mathrm{GHz}$), Wi-Max (3.4–$3.6\,\mathrm{GHz}$), Sub-6 GHz 5G (3.3–$4.2\,\mathrm{GHz}$), and WLAN (5.15–$5.825\,\mathrm{GHz}$). The antenna also provides safe SAR value, low envelope correlation coefficient, good antenna gain, acceptable radiation efficiency, optimum Total Active Reflection Coefficient (TARC) value, low Channel Capacity Loss (CCL), good gain, and acceptable radiation efficiency across the frequency ranges. Simulated and measured performances of the antenna in the entire band are presented.

1. INTRODUCTION

Recent years have seen significant progress in the development and production of flexible, electrical widgets due to the widespread use of wearable devices. Wearable, flexible electronic goods offer a larger range of uses than their rigid counterparts because they are more compact, flexible, robust, and adaptable in nature [1, 2].

One of the most widely conducted research in the field of human-centered communication antennas is the study of wearable or flexible antennas. Soldiers, the elderly, patients, and athletes can all benefit from constant monitoring through Personal Area Networks (PAN) or Body Area Networks (BAN) made possible by wearable antennas. As the field of wireless communications evolves, researchers and developers have begun to focus increasingly on Multiple-Input Multiple-Output (MIMO) techniques for the use in the next generation of devices [3, 4]. In the coming years, handheld electronics will have to incorporate large number of MIMO transceivers. Due to space constraints, it can be challenging to implement optimal configurations for numerous antennas in handheld devices [5, 6]. In order to minimize mutual coupling among MIMO antenna elements, orthogonal structure is employed in these antenna designs [7]. MIMO antennas for telecommunications are observed in [8] which use a common ground and coplanar waveguide (CPW) feeding.

When it comes to MIMO antenna configurations for wearable applications, the available literature is very few. There are reports of a dual-band textile MIMO antenna [9] and a decoupled UWB MIMO antenna [10]. Fabric substances are used in the construction of neutralization line-based UWB MIMO antennas for wearable devices [9–11], which leads to substantial foot-traces and system failures due to deformation, denting, and environmental impacts. Ground radiation MIMO antenna with polarization diversity performance [12], antenna configuration consisting of a ring co-radiator with a high impedance

[1] Department of Electronics, Cochin University of Science & Technology, Kerala, India. [2] ACARR, Cochin University of Science & Technology, Kerala, India.

surface [13], and MIMO antennas that are in the form of an octagonal ring with four elements are reported [14].

The parametric studies on antenna structure configuration have been carried out in order to reach the optimal prototype. The purpose of these studies is to give the best antenna model with the intention of keeping fabrication inconsistencies as small as possible while maintaining a high isolation quality across a wide operation frequency range. The similar effect may be obtained by paying close attention to the design of the associated ground plane lines and by including slots into the substrate. The characteristics of a MIMO antenna are estimated in terms of Envelope Correlation Coefficient (ECC), Diversity Gain (DG), and all of the numerically estimated and empirically determined findings must be in accordance with ideal values specified in operating standards under circumstances as recommended in [15–17].

As the frequency range of 3.1 GHz to 9.3 GHz is envisioned for the proposed antenna, it is expected to cater different fields of wireless communication.

2. UNIT ANTENNA GEOMETRY, DESIGN AND THEORY

For the suggested antenna, an FR4 substrate with a thickness of 0.07 mm is chosen. FR4 sheets are electrical insulators with high dielectric strength and high strength-to-weight ratio. This material is also known to have good relative temperature resistance and can perform well in most environmental conditions [18].

The unit antenna to be used as the element in the quad element MIMO antenna is designed at first. Fig. 1 depicts the structure and radiation characteristic of the unit antenna. The design comprises a rectangular patch containing a metamaterial inspired impedance resonator structure fed using a coplanar
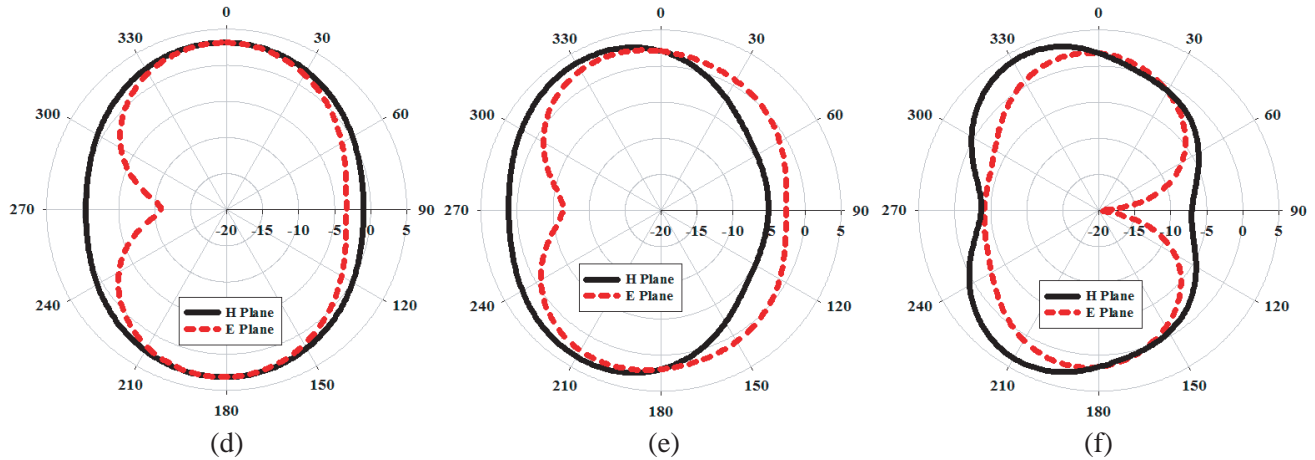

(a)

(b)

(c)
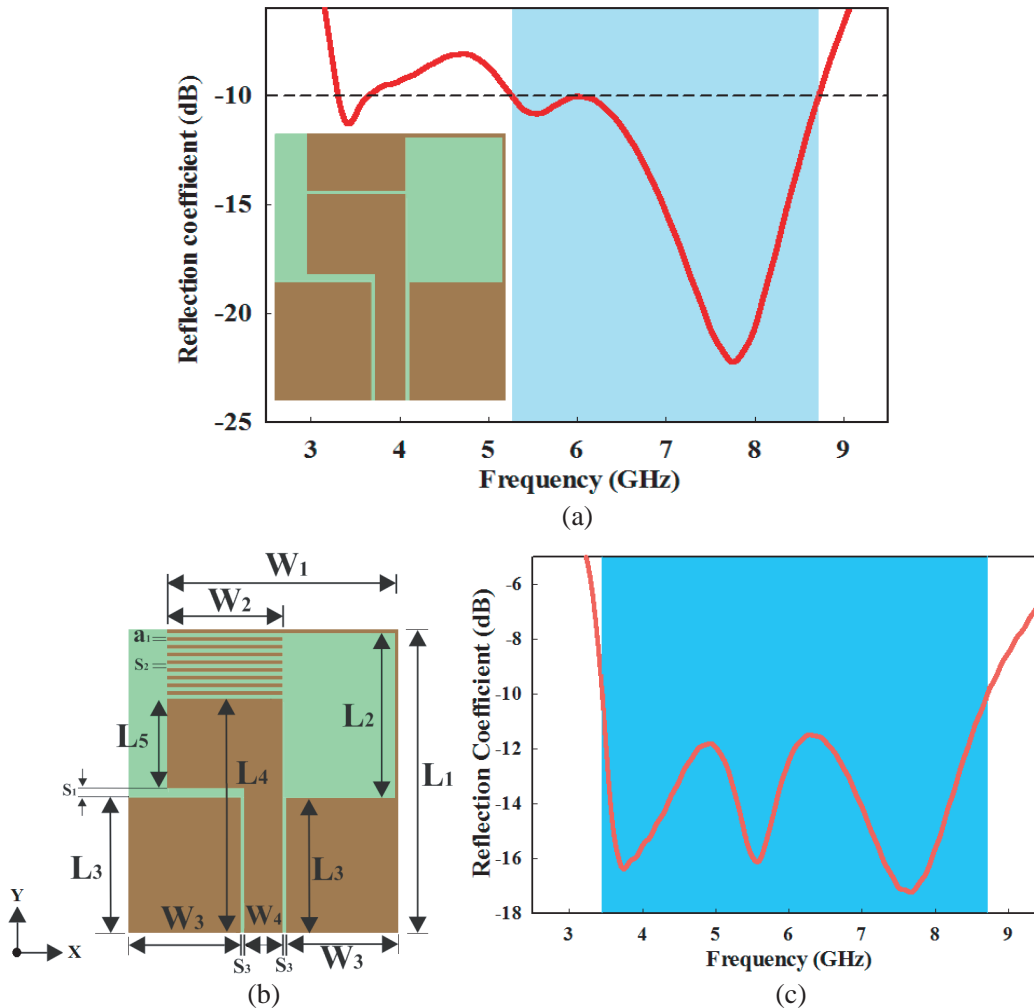
Figure 1. (a) Schematic view of unit antenna without intermittent impedance structure. (b) Schematic view of proposed single antenna unit. (c) Simulated S_{11} of the unit antenna. (d) Two-dimensional radiation pattern. At (d) 3.7 GHz, (e) 5.5 GHz, (f) 7.6 GHz.

waveguide. Fig. 1(b) presents the optimized geometry and Fig. 1(c) the variation of reflection coefficient with the frequency. The unit antenna shows a wide bandwidth with resonances at frequencies 3.7 GHz, 5.5 GHz, and 7.6 GHz. Figs. 1(d), (e), (f) show the far field radiation pattern at aforesaid frequencies. As can be seen from the plots, the radiation in both planes is almost omnidirectional.

In order to enhance the impedance properties of the antenna, an intermittent spaced metamaterial inspired impedance structure has been included in the microstrip patch. Fig. 1(a) depicts the unit antenna structure without intermittent structures in the radiating patch. Intermittently spaced impedance structure enhances the bandwidth of the suggested antenna almost by 2 GHz. Intermittent spaces present in the impedance structure are thus optimized to improve the bandwidth. The optimal structural parameters of the antenna are shown in Table 1. Fig. 2 shows the dispersion of the surface currents from feedline to the radiating patch for resonant frequencies 3.3, 5.8, and 8.5 GHz, respectively.

Table 1. Structural dimensions of the unit antenna.

Parameter	Value (mm)	Parameter	Value (mm)
L_1	14	S_2	1.0
L_2	17.5	S_3	0.35
L_3	9.3	W_1	24
a	0.4	W_2	4.0
S_1	0.35	W_3	12.0

3. INTEGRATION OF FOUR ELEMENT MIMO ANTENNA

The antenna elements are arranged orthogonally at an end-to-end spacing of $W_4 = 5$ mm as shown in Fig. 3(a) which is useful for exploiting polarization diversity [19]. Because of the orthogonal field generated by the neighboring radiating units, significant isolation is attained [20]. Now, the grounds of antenna elements are connected using transmission lines through rectangular lines of width 0.4 mm as shown in Fig. 3. The presence of these ground lines further reduces the coupling and improves the isolation.

Figures 3(a) & (b) show the schematic of the resultant structure of the quad element MIMO antenna. The bottom side of the MIMO antenna includes small conducting patches of dimension $L_s = 7$ mm and $W_s = 5$ mm. It is arranged below the gaps between the unit antennas as shown.
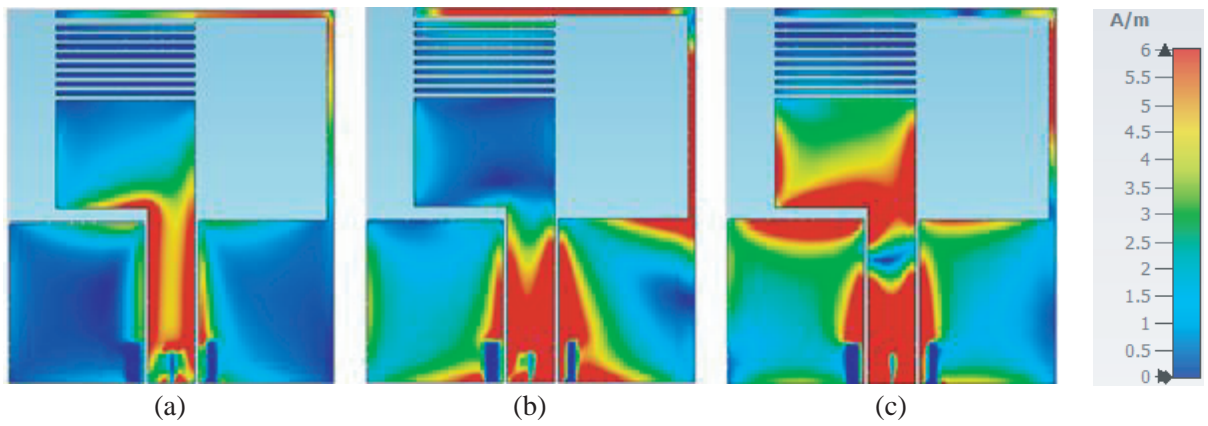
Figure 2. Simulated surface current distributions of the proposed antenna for (a) 3.3 GHz, (b) 5.8 GHz and (c) 8.5 GHz.
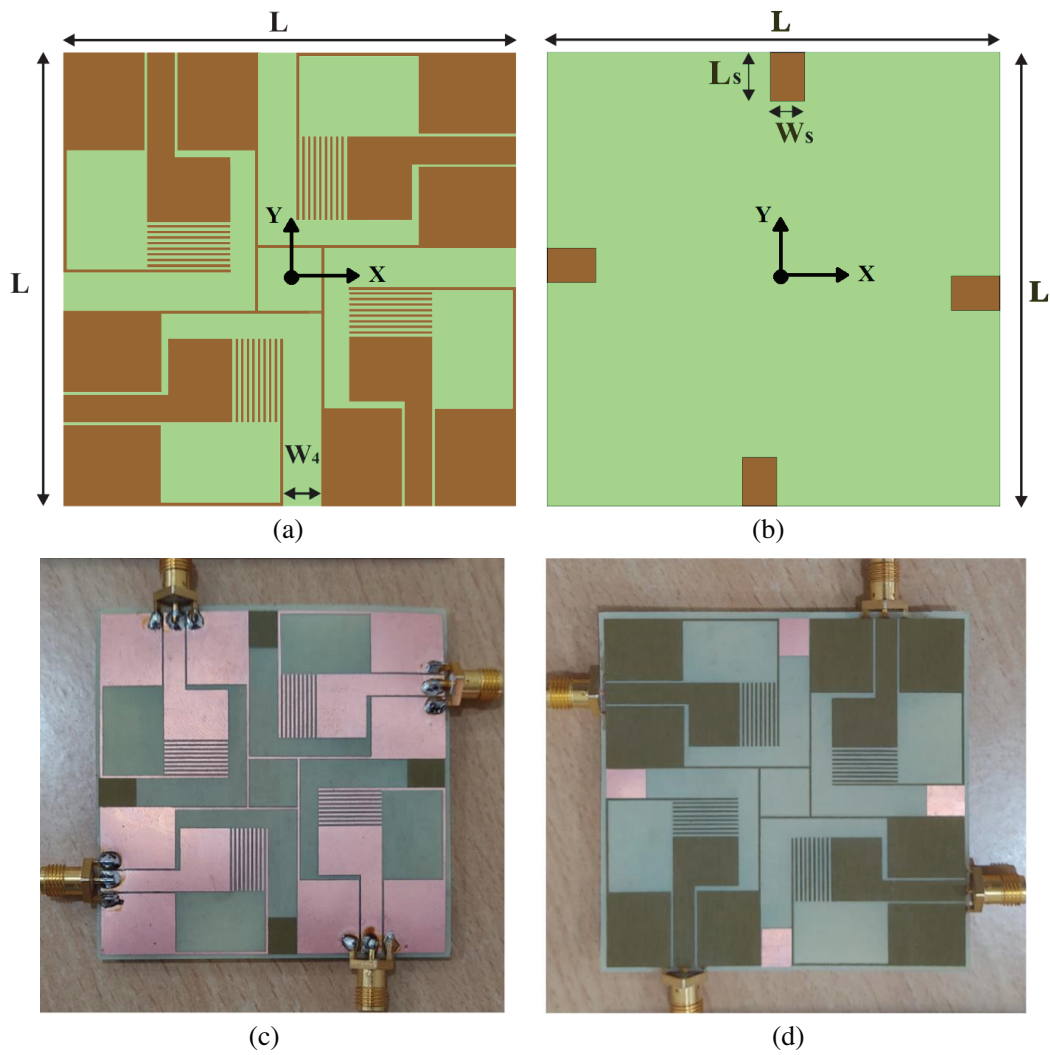

Figure 3. Schematic of the four-element MIMO antenna. (a) Top view. (b) Bottom view. (c) Fabricated MIMO antenna-top view. (d) Bottom view.

This arrangement gives better matching and impedance bandwidth. The optimal dimensions for the complete antenna are $65\,\text{mm} \times 65\,\text{mm} \times 0.07\,\text{mm}$. Figs. 3(c) & (d) show photographs of the fabricated MIMO antenna.

3.1. Impedance Performance

Figure 4(a) depicts a chart of the reflection coefficient vs the frequency. The measured $-10\,\text{dB}$ impedance bandwidth of the antenna is in the range $3.1\,\text{GHz}$ to $9.3\,\text{GHz}$. Fig. 4(b) shows the measured isolation (S_{12}, S_{13}, and S_{14}) values for the quad-element MIMO antenna. It can be shown that the isolation value is more than $17\,\text{dB}$ throughout the band.
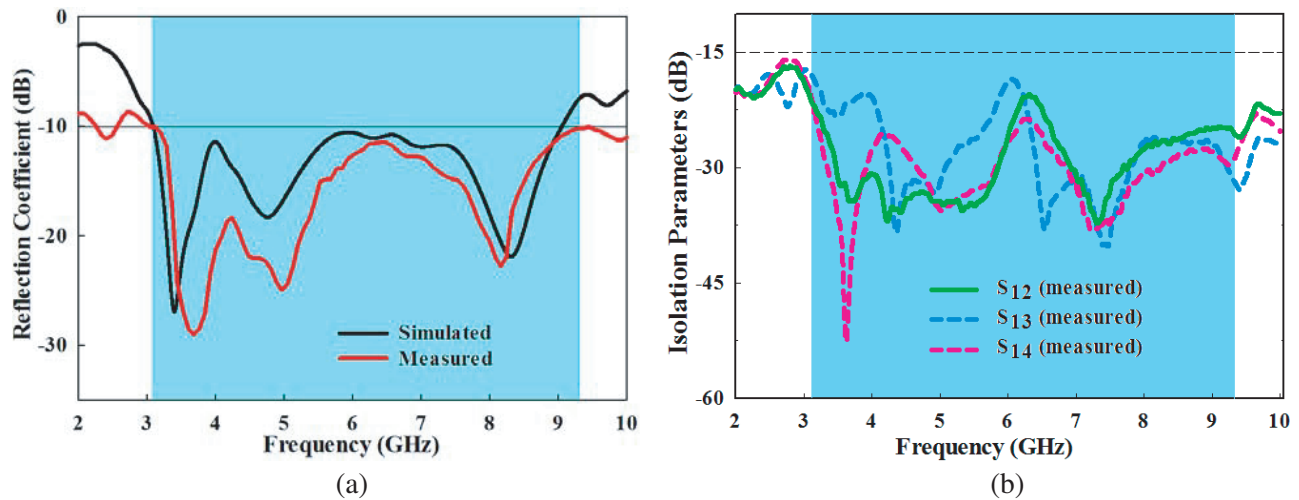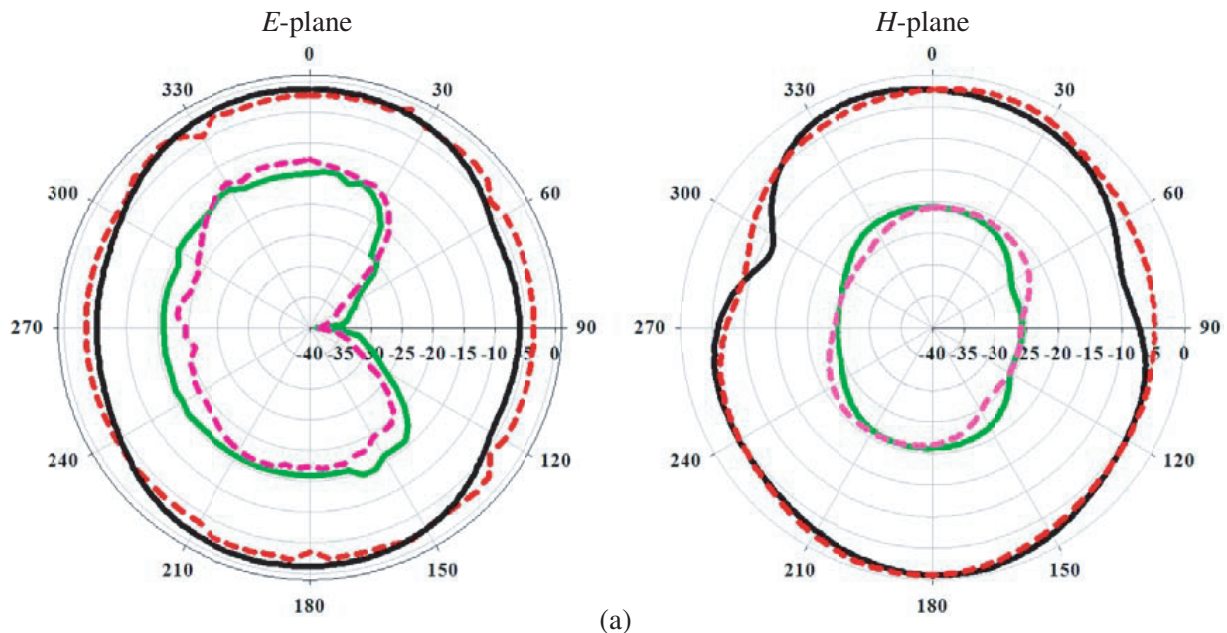

Figure 4. (a) Simulated and measured reflection characteristics of the 4 port antenna. (b) Measured isolation parameters of the 4 port antenna.

3.2. Radiation Performance

2D radiation patterns at different frequencies are given in Fig. 5. The pattern is almost omnidirectional with slight distortion at some frequencies.
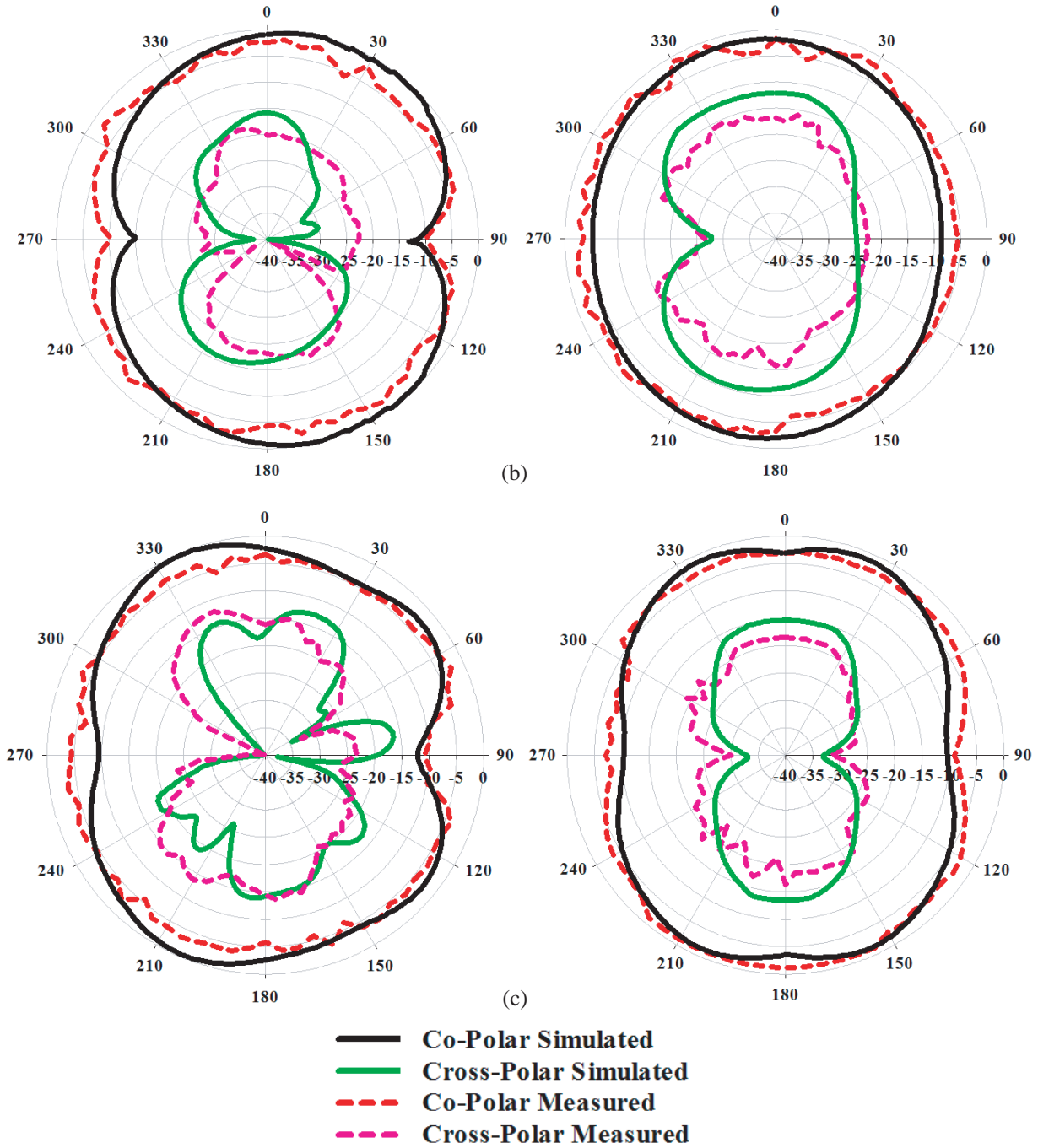
Figure 5. Measured and simulated two-dimensional radiation pattern. (a) 3.6 GHz. (b) 4.9 GHz. (c) 8.1 GHz.

Figure 6 shows the measured gain and radiation efficiency data. Measured maximum gain is 5.9 dB (at 6.7 GHz), with a radiation efficiency of more than 50% throughout operational bandwidth, with values reaching more than 65% at some frequency points.

3.3. Diversity Capabilities of Four-Element MIMO Antenna

As a consequence of the close proximity of antenna components, designing the MIMO antenna is a difficult challenge. The port coupling and field coupling increase as a result. These couplings have an
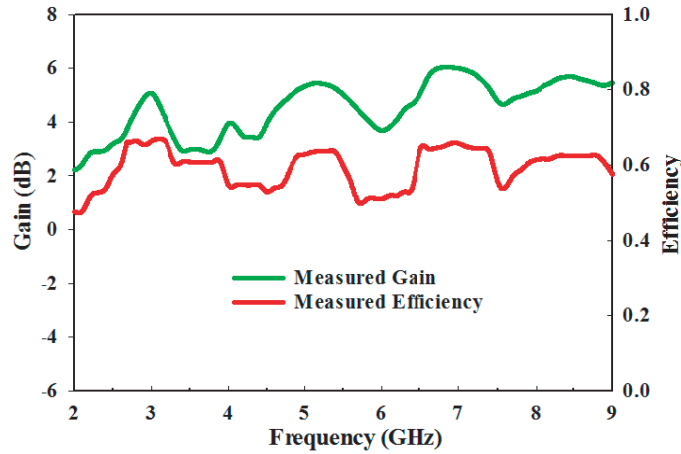
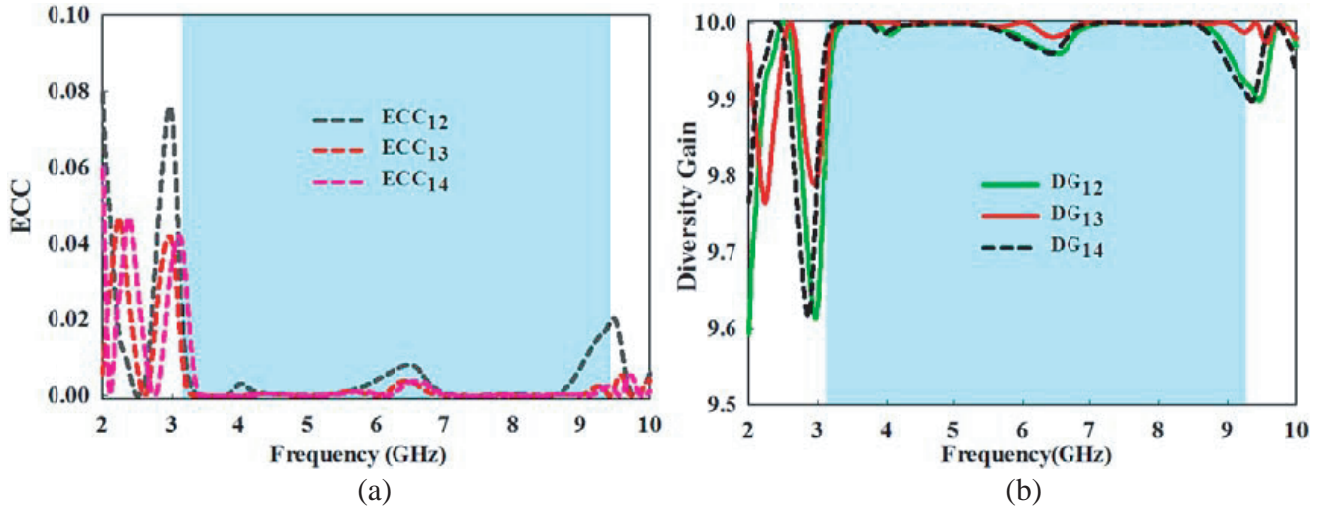**Figure 6.** Gain and efficiency of the antenna.

Figure 7. The suggested MIMO antenna's diversity performance. (a) ECC. (b) DG.

impact on the proposed antenna efficiency and channel capacity [25]. As a result, there is a need for good isolation and low correlation level. The suggested MIMO antenna's performance characteristics, such as ECC, DG, Total Active Reflection Coefficient (TARC), and Channel Capacity Loss (CCL), are determined, as shown in Figs. 7(a) & (b) and 8(a) & (b).

The suggested MIMO antenna's measured ECC (ρ_{12}, ρ_{13}, and ρ_{14}) is presented in Fig. 7(a) using Eq. (3). The measured ECC of the proposed MIMO antenna is less than 0.05 for the whole operating band, indicating good diversity performance. The proposed MIMO antenna's measured DG plot is displayed in Fig. 7(b), which is derived using Eq. (4). The developed antenna's DG ranges between 9.95 and 9.99 guaranteeing good performance. According to Fig. 7(b), the DG for the working band is about equal to 10.

$$\rho_{ij} = \frac{-S_{ii}S_{ij}^* - S_{ji}S_{jj}^*}{\sqrt{(1 - |S_{ii}|^2 - |S_{ji}|^2)(1 - |S_{jj}|^2 - |S_{ij}|^2)_{ij}}} \tag{1}$$

$$DG = 10 \times \sqrt{1 - |ECC|} \tag{2}$$

where ρ_{ij} is the correlation coefficient between antenna elements i and j; S_{ij} is the transmission coefficient between antenna elements i and j; and η_i and η_j are the radiation efficiencies of antenna elements i and j, respectively.
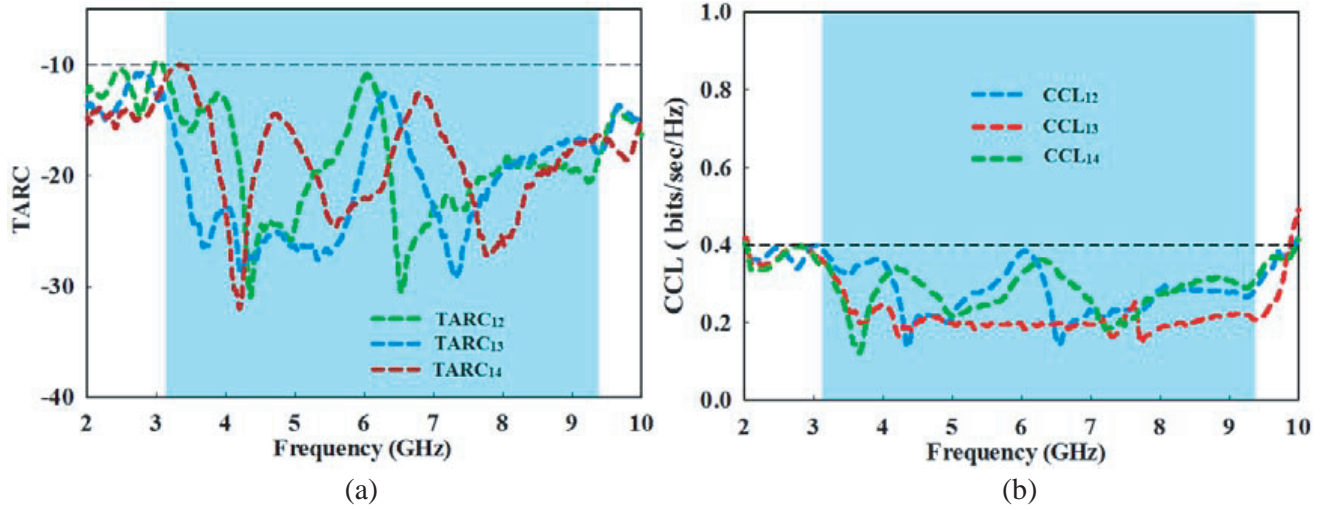
Figure 8. The suggested MIMO antenna's diversity performance. (a) TARC, and (b) CCL.

The measured results of TARC derived using Eq. (5) are shown in Fig. 8(a). The TARC values are found to be less than $-10\,\text{dB}$ for all phase values. According to Fig. 8(b), the suggested four-element MIMO design has an extremely low CCL value [estimated using Eqs. (6) to (8)] of less than $0.4\,\text{bits/s/Hz}$, which is much less than the allowed limit of $0.4\,\text{bits/s/Hz}$ for the operating region [25].

$$\Gamma_a^t = \sqrt{\frac{|S_{11} + S_{12}e^{j\theta}|^2 + |S_{21} + S_{22}e^{j\theta}|^2}{2}} \tag{3}$$

$$CC_{loss} = -\log_2\left|\varphi^R\right|, \quad \text{where} \quad \varphi^R = \begin{bmatrix} \varphi_{11} & \varphi_{12} \\ \varphi_{21} & \varphi_{22} \end{bmatrix} \tag{4}$$

$$\varphi_{11} = 1 - \left(|S_{11}|^2 + |S_{12}|^2\right), \quad \varphi_{22} = 1 - \left(|S_{22}|^2 + |S_{21}|^2\right) \tag{5}$$

$$\varphi_{12} = -\left(S_{11}^* S_{12} + S_{21}^* S_{22}\right), \quad \varphi_{21} = -\left(S_{22}^* S_{21} + S_{12}^* S_{11}\right) \tag{6}$$

To evaluate the effectiveness of the proposed MIMO antenna, it is compared to the existing flexible antennas in Table 2. The suggested MIMO antenna strikes a great balance among electric size, thickness, radiation efficiency, bandwidth, isolation, and ECC compared to the antennas in [26–34].

3.4. Bending Analysis

For reliable operation on conformal surfaces, it is crucial to understand how the proposed flexible MIMO antenna's performance changes due to bending of the structure. Therefore, bending analysis is used to verify performance characteristics of the bent MIMO. The antenna is then placed on a cylindrical block of Styrofoam ($\varepsilon_r = 1.03$) of diameter $50\,\text{mm}$. The scattering parameters are measured after bending along x axis as in [21]. Fig. 9(a) illustrates the measured scattering parameters for the bent antenna. Fig. 9(b) depicts the bending process on a Styrofoam cylinder, along x axis.

An impedance bandwidth (3.4 to $9.1\,\text{GHz}$) similar to that of the unbent MIMO antenna (3.1 to $9.3\,\text{GHz}$) is observed along X-axis bending. Since the MIMO antenna is identical along X and Y axes, a similar result is expected along Y axis. Since the port isolation values are larger than $15\,\text{dB}$ in Fig. 9(a), the MIMO antenna performance isolation requirements are met.

Figures 10(a), (b), & (c) show the measured ECC, DG, and TARC values under the bending configuration. Fig. 10(a) illustrates that ECC value is well below 0.1 in the whole operative band. This value has to be less than or equal to 0.3 in order to ensure that MIMO applications function to their full potential [15]. When gauging the reliability of MIMO antennas, diversity gain (DG) is another crucial metric to take into account. Fig. 10(b) illustrates DG in bending condition. Under bending along X-axis, DG is found to be greater than 9.85. It is a good indication of the MIMO
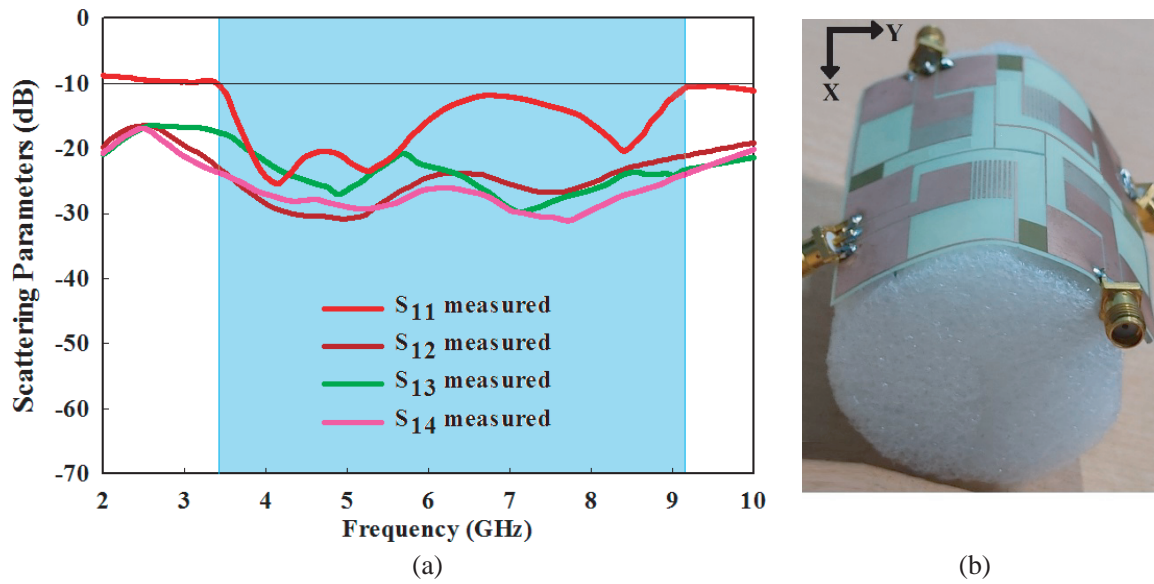
Figure 9. (a) Measured S parameters of the flexible MIMO antenna for bending along X-axis. (b) MIMO antenna on a Styrofoam bent along X-axis.

Table 2. Analysis of proposed work with similar existing flexible antennas from literature.

| Ref. No.	Electric Size	Thickness (mm)	IBW (GHz)	Radiation Efficiency	Isolation (dB)	ECC	Material
[26]	40×40	1.124	2.4–2.48, 5.15–5.8	43%, 46%	> 15	–	Micrometal mesh film glued on a glass substrate
[27]	22×31	0.125	3.43–10.1	63%	> 15	< 0.3	Kapton polyimide substrate
[28]	126×70	4.27	5.6–6.1	72%	> 30	0.001	multilayered polydimethylsiloxane (PDMS) substrate
[29]	38.1×38.1	2	2.4–2.5	27%	> 12	< 0.01	Conductive copper Felt substrate
[30]	180×180	1.52	2.6–3.18, 5.3–6.06, 6.7–6.94	70%	13	< 0.5	Thick flexible Rogers RO3003
[31]	31.6×3.3	0.5	33.8–36.1	–	> 40	–	RT/duroid5880
[32]	11×25.4	0.147	27.2–40	–	> 20	< 0.06	Silver nanoparticle ink
[33]	60×60	0.2	4.4–5	85%	> 20	< 0.005	Ni based embedded metallic mesh
[34]	66×45	0.625	2.21–6	41%	> 15	< 0.016	AgHT-4 Malinex (ST507)
Proposed Work	65×65	0.07	3–9.3	50%	> 15	< 0.08	Thin FR-4 film
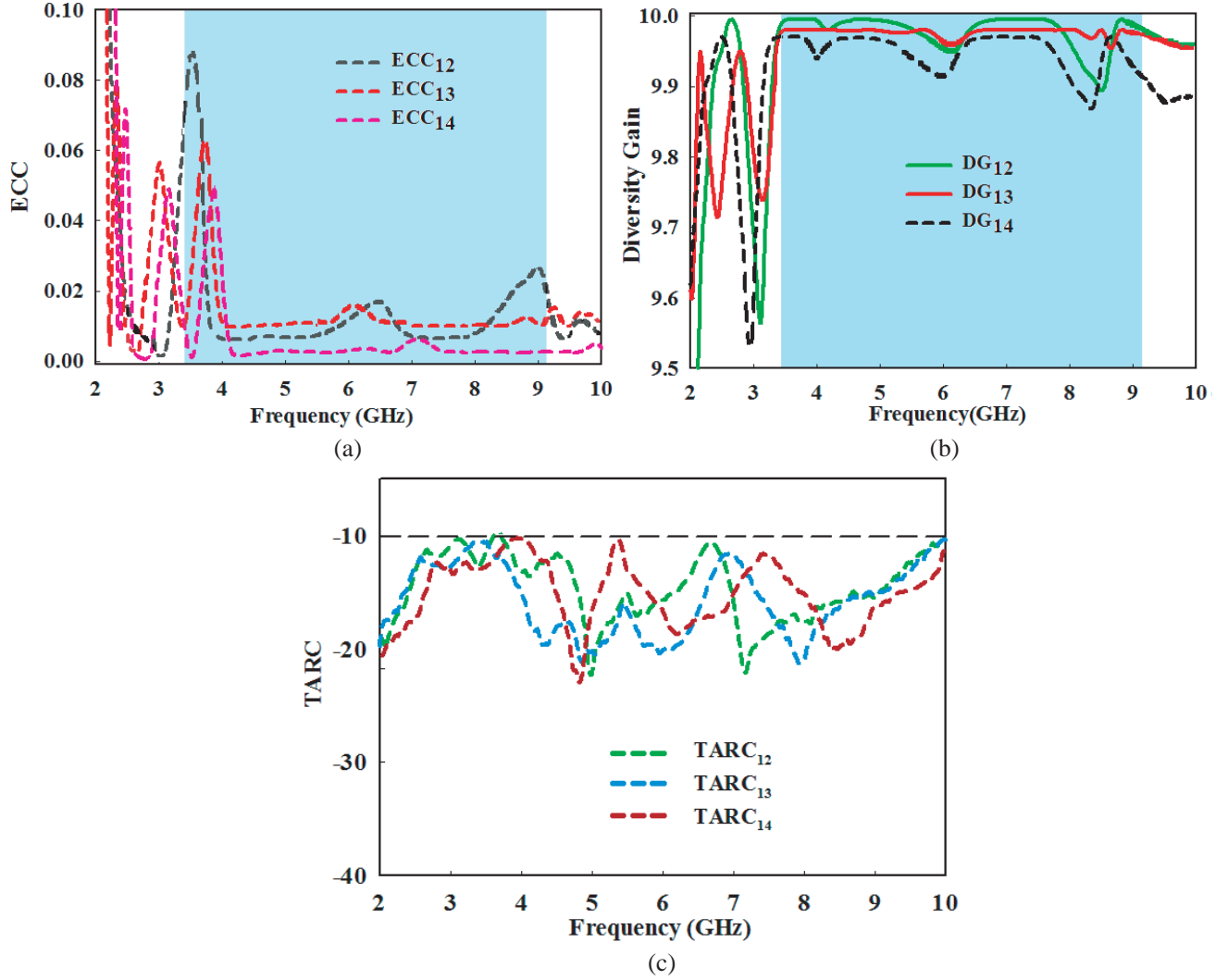
Figure 10. (a) Measured ECC of the MIMO antenna for bending along X-axis. (b) Measured DG after bending along X-axis. (c) Measured TARC of the MIMO for bending along X-axis.

system's dependability and diversity performance. TARC values of bent MIMO antenna are illustrated in Fig. 10(c). TARC value is below -10 dB, and therefore MIMO performance requirements are met even under bent conditions.

3.5. SAR Analysis

On-body technologies need the use of wearable textile antennas, which necessitates that the antenna function in close proximity to human body. Thus, Specific Absorption Ratio (SAR) must be computed once the antenna is activated on the body. Normal units for describing SAR values are expressed in W/kg. SAR is a method of calculating how much energy a body absorbs from radio waves. Electric field and SAR have a one-to-one relationship. It is possible to determine the SAR (W/kg) given the electric field, **E** (V/m), conductivity of the material, σ (S/m), and the density of the material, ρ (kg/m^3) [22].

$$\text{SAR} = \frac{\sigma \times \text{E}^2_{\text{RMS}}}{\rho} \tag{7}$$

$$\text{E}^2_{\text{RMS}} = \text{incident power density (s)} \times 377 \tag{8}$$

A $150 \times 150 \times 40\,\text{mm}^3$ cuboid is used to model human organs for the purpose of studying the effect on multilayer tissues. Muscle, fat, and skin make up the model's three distinct layers. Table 3 provides approximate value for mass density, thickness, conductivity, and permittivity for each layer. Its properties are taken according to [23] and are enumerated in Table 3.

Table 3. Characteristics of human tissues for 4 GHz.

Tissue	Thickness (mm)	Conductivity (S/m)	Permittivity
Skin	2	2.34	36.5
Fat	4	0.18	5.1
Muscle	10	3.01	50.8

The multilayer model simulation result is shown in Fig. 11. The prototype is positioned 1 mm behind the proposed antenna. The antenna's input power is set to 100 mW, and the software in the CST MWS uses the IEEE C95.1 standards to calculate the SAR results. The IEEE C95.1 standard states that the SAR value of a device has to be lower than 2 W/kg when being averaged across 10 g of tissue in a cube form [24]. The SAR levels at 3.39 GHz, 4.75 GHz, and 8.1 GHz are found at 1.29 W/kg, 1.47 W/kg, and 1.71 W/kg, respectively. The obtained value is below the safety limit of 2 W/kg.
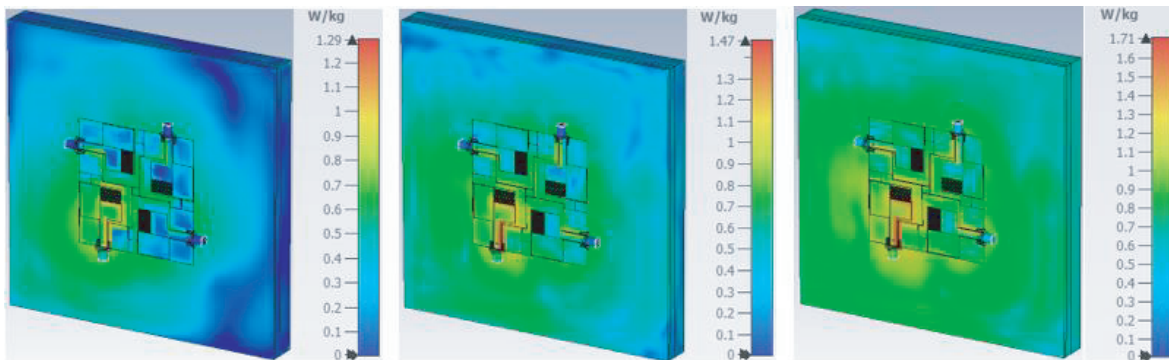

Figure 11. Obtained SAR values as per IEEE C95.1 standards.

4. CONCLUSION

The purpose of this work is observing the functionality of the suggested antenna for UWB applications and other wireless communication applications like ISM, Wi-Fi, and WiMAX, W-LAN, Sub-6 GHz 5G, etc. The designed flexible and wearable antenna has a good performance over the whole bandwidth it occupies. The most important discovery made by this research is the fact that the proposed UWB MIMO antenna may be utilized for a variety of applications in 5G, S, C, and X bands. The novel self-decoupled MIMO antennas are inherently segregated across broad frequency range without the need for external decoupling devices. The suggested design scheme shows remarkable possibilities for the development of highly integrated MIMO antennas for 5G devices in the future due to its straightforward structure, expansive bandwidth, and high efficiency.

In order to verify the idea, the simulation of the 2×2 MIMO antenna system is followed by fabrication and measurement of its performance. Both the antenna's operating mechanism and its performance are investigated. In general, results of both the simulation and experiment match well. Furthermore, the findings of the SAR simulation demonstrate that the antenna satisfies the safety standards. Because of its adaptability and wide frequency range, this antenna might be used in a variety of wearable electronics.

ACKNOWLEDGMENT

REFERENCES

1. Ho, C. D., T.-V. Nguyen, T. Huynh-The, T.-T. Nguyen, D. B. da Costa, and B. An, "Short-packet communications in wireless-powered cognitive IoT networks: Performance analysis and deep learning evaluation," *IEEE Trans. Veh. Technol.*, Vol. 70, 2894–2899, 2021.

2. Kamalaveni, A. and M. Ganesh Madhan, "A compact TRM antenna with high impedance surface for SAR reduction at 1800 MHz," *AEU — Int. J. Electron. Commun.*, Vol. 70, 1192–1198, 2016.

3. Razzaqi, A. A., B. A. Khawaja, and M. Ramzan, "A triple-band antenna array for next-generation wireless and satellite-based applications," *International Journal of Microwave and Wireless Technologies*, Vol. 8, 71–80, Feb. 2016.

4. Patel, S. S., I. J. Zuazola, and W. G. Whittow, "Antenna with three dimensional 3D printed substrates," *Microwave and Optical Technology Letters*, Vol. 58, 741–744, Apr. 2016.

5. Guan, D. F., Y. S. Zhang, Z. P. Qian, and Y. Li, "Compact microstrip patch array antenna with parasitically coupled feed," *IEEE Transactions on Antennas and Propagation*, Vol. 64, 2531–2534, Jun. 2016.

6. Wei, K., J. Y. Li, L. Wang, and Z. J. Xing, "Mutual coupling reduction by novel fractal defected ground structure bandgap filter," *IEEE Transactions on Antennas and Propagation*, Vol. 64, 4328–4335, Oct. 2016.

7. Foudazi, A., M. T. Ghasr, and K. M. Donnell, "Mutual coupling in aperture-coupled patch antennas by orthogonal SIW line," *IEEE International Symposium on Antennas and Propagation (APSURSI)*, 1587–1588, 2016.

8. Zhao, N. and W.-P. Tian, "CPW-fed dual-band MIMO antenna with common radiating element," *Progress In Electromagnetics Research Letters*, Vol. 62, 71–75, Sep. 2016.

9. Yan, S., P. J. Soh, and G. A. E. Vandenbosch, "Dual-band textile MIMO antenna based on Substrate Integrated Waveguide (SIW) technology," *IEEE Transactions on Antennas and Propagation*, Vol. 63, 4640–4647, 2015.

10. Biswas, A. K. and U. Chakraborty, "Compact wearable MIMO antenna with improved port isolation for ultra-wideband applications," *IET Microwaves, Antennas & Propagation*, Vol. 13, 498–504, 2019.

11. Biswas, A. K. and U. Chakraborty, "Investigation on decoupling of wideband wearable multiple-input multiple output antenna elements using microstrip neutralization line," *RF and Microwave Computer Aided Engineering*, Vol. e21723, 1–11, 2019.

12. Qu, L., H. Piao, Y. Qu, H. Kim, and H. Kim, "Circularly polarised MIMO ground radiation antennas for wearable devices," *IET Electronics Letters*, Vol. 54, 189–190, 2018.

13. Wen, D., Y. Hao, M. O. Munoz, H. Wang, and H. Zhou, "A compact and low-profile MIMO antenna using a miniature circular high-impedance surface for wearable applications," *IEEE Transactions on Antennas and Propagation*, Vol. 66, No. 1, 96–104, 2018.

14. Chouhan, S., D. K. Panda, P. K. Khushwah, and P. K. Mishra, "Octagonal-shaped wideband MIMO antenna for human interface device and S-band application," *International Journal of Microwave and Wireless Technologies*, Vol. 11, 287–296, 2019.

15. Pannu, P. and D. K. Sharma, "Miniaturize four-port UWB-MIMO antenna with tri-notched band characteristics," *Microwave and Optical Technology Letters*, Vol. 63, No. 5, 1489–1498, May 2021.

16. Ibrahim, A. A. and A. E. Ali, "High isolation 4-element ACS-fed MIMO antenna with band notched feature for UWB communications," *Int. J. Microw. Wireless Technol.*, Vol. 69, 1–11, Feb. 2021.

17. Desai, A., J. Kulkarni, M. M. Kamruzzaman, Š. Hubálovský, H.-T. Hsu, and A. A. Ibrahim, "Interconnected CPW fed flexible 4-port MIMO antenna for UWB, X, and Ku band applications," *IEEE Access*, Vol. 10, 57641–57654, 2022.

18. Varadhan, C., S. Arulselvi, and F. A. Chamatu, "Effects of the FR 4 substrate realized in a circularly polarized UHF-RFID reader antenna with fractal geometry for enhancing parameters," *Advances in Materials Science and Engineering*, Vol. 2021, Article ID 8475621, 7 pages, 2021.

19. Elobied, A. A., X.-X. Yang, N. Xie, and S. Gao, "Dual-band 2×2 MIMO antenna with compact size and high isolation based on half-mode SIW," *International Journal of Antennas and Propagation*, Vol. 2020, Article ID 2965767, 11 pages, 2020.

20. Kumar, P., S. Urooj, and F. Alrowais, "Design and implementation of quad-port MIMO antenna with dual-band elimination characteristics for ultra-wideband applications," *Appl. Sci.*, Vol. 10, 1715, 2020.

21. Ashyap, A. Y. I., et al., "Highly efficient wearable CPW antenna enabled by EBG-FSS structure for medical body area network applications," *IEEE Access*, Vol. 6, 77529–77541, 2018.

22. Mu, G. and P. Ren, "A compact dual-band metasurface-based antenna for wearable medical body-area network devices," *Journal of Electrical and Computer Engineering*, Vol. 2020, Article ID 4967198, 10 pages, 2020.

23. Liao, C.-T., Z.-K. Yang, and H.-M. Chen, "Multiple integrated antennas for wearable fifth-generation communication and internet of things applications," *IEEE Access*, Vol. 9, 120328–120346, 2021.

24. IEEE Std. C95.1 (2005) IEEE standard for safety levels with respect to human exposure to the radio frequency electromagnetic fields 3 kHz to 300 GHz.

25. Ameen, M., O. Ahmad, and R. K. Chaudhary, "Bandwidth and gain enhancement of triple-band MIMO antenna incorporating metasurface based reflector with for WLAN/WiMAX applications," *IET Microwave, Antenna Propag.*, Vol. 14, No. 13, 1493–1503, Oct. 2020.

26. Li, Q. L., S. W. Cheung, D. Wu, and T. I. Yuk, "Optically transparent dualband MIMO antenna using micro-metal mesh conductive film for WLAN system," *IEEE Antennas Wireless Propag. Lett.*, Vol. 16, 920–923, 2017.

27. Li, W., Y. Hei, P. M. Grubb, X. Shi, and R. T. Chen, "Compact inkjetprinted flexible MIMO antenna for UWB applications," *IEEE Access*, Vol. 6, 5029–50298, 2018.

28. Alqadami, A. S. M., M. F. Jamlos, P. J. Soh, and G. A. Vandenbosch, "Assessment of PDMS technology in a MIMO antenna array," *IEEE Antennas Wireless Propag. Lett.*, Vol. 15, 1939–1942, 2016.

29. Li, H., S. Sun, B. Wang, and F. Wu, "Design of compact single-layer textile MIMO antenna for wearable applications," *IEEE Transactions on Antennas and Propagation*, Vol. 66, No. 6, 3136–3141, Jun. 2018.

30. Jha, K. R., Z. A. P. Jibran, C. Singh, and S. K. Sharma, "4-port MIMO antenna using common radiator on a flexible substrate for sub-1 GHz, sub-6 GHz 5G NR, and Wi-Fi 6 applications," *IEEE Open J. Antennas Propag.*, Vol. 2, 689–701, 2021.

31. Wang, Q., N. Mu, L. Wang, S. Safavi-Naeini, and J. Liu, "5G MIMO conformal microstrip antenna design," *Wireless Commun. Mobile Comput.*, Vol. 2017, Art. No. 7616825, Dec. 2017.

32. Jilani, S. F., A. Rahimian, Y. Alfadhl, and A. Alomainy, "Low-profile flexible frequency-reconfigurable millimetre-wave antenna for 5G applications," *Flexible Printed Electron.*, Vol. 3, No. 3, Art. No. 035003, 2018.

33. Qiu, H., H. Liu, X. Jia, Z.-Y. Jiang, Y.-H. Liu, J. Xu, T. Lu, M. Shao, T.-L. Ren, and K. J. Chen, "Compact, flexible, and transparent antennas based on embedded metallic mesh for wearable devices in 5G wireless network," *IEEE Transactions on Antennas and Propagation*, Vol. 69, No. 4, 1864–1873, Apr. 2021.

34. Desai, A., M. Palandoken, J. Kulkarni, G. Byun, and T. K. Nguyen, "Wideband flexible/transparent connected-ground MIMO antennas for sub-6 GHz 5G and WLAN applications," *IEEE Access*, Vol. 9, 147003–147015, 2021.